Inflammation in the hippocampus affects IGF1 receptor signaling and contributes to neurological sequelae in rheumatoid arthritis

Karin M. E. Andersson[a,1,2], Caroline Wasén[a,1], Lina Juzokaite[a], Lovisa Leifsdottir[a,b], Malin C. Erlandsson[a,b], Sofia T. Silfverswärd[a], Anna Stokowska[c], Marcela Pekna[c], Milos Pekny[c], Kjell Olmarker[d], Rolf A. Heckemann[e,f,g], Marie Kalm[h], and Maria I. Bokarewa[a,b,2]

[a]Department of Rheumatology and Inflammation Research, Institute of Medicine, University of Gothenburg, 40530 Gothenburg, Sweden; [b]Rheumatology Clinic, Sahlgrenska University Hospital, 41346 Gothenburg, Sweden; [c]Center for Brain Repair and Rehabilitation, Department of Clinical Neuroscience, Institute of Neuroscience and Physiology, University of Gothenburg, 40530 Gothenburg, Sweden; [d]Musculoskeletal Research, Department of Medical Chemistry and Cell Biology, Institute of Biomedicine, University of Gothenburg, 40530 Gothenburg, Sweden; [e]Med Tech West, Sahlgrenska University Hospital, 41345 Gothenburg, Sweden; [f]Department of Medical Radiation Science, Sahlgrenska University Hospital, 41345 Gothenburg, Sweden; [g]Faculty of Medicine, Imperial College London, London SW7 2AZ, United Kingdom; and [h]Department of Pharmacology, Institute of Neuroscience and Physiology, University of Gothenburg, 40530 Gothenburg, Sweden

Edited by Bruce McEwen, The Rockefeller University, New York, NY, and approved October 24, 2018 (received for review June 19, 2018)

Rheumatoid arthritis (RA) is an inflammatory joint disease with a neurological component including depression, cognitive deficits, and pain, which substantially affect patients' quality of daily life. Insulin-like growth factor 1 receptor (IGF1R) signaling is one of the factors in RA pathogenesis as well as a known regulator of adult neurogenesis. The purpose of this study was to investigate the association between IGF1R signaling and the neurological symptoms in RA. In experimental RA, we demonstrated that arthritis induced enrichment of IBA1$^+$ microglia in the hippocampus. This coincided with inhibitory phosphorylation of insulin receptor substrate 1 (IRS1) and up-regulation of IGF1R in the pyramidal cell layer of the cornus ammoni and in the dentate gyrus, reproducing the molecular features of the IGF1/insulin resistance. The aberrant IGF1R signaling was associated with reduced hippocampal neurogenesis, smaller hippocampus, and increased immobility of RA mice. Inhibition of IGF1R in experimental RA led to a reduction of IRS1 inhibition and partial improvement of neurogenesis. Evaluation of physical functioning and brain imaging in RA patients revealed that enhanced functional disability is linked with smaller hippocampus volume and aberrant IGF1R/IRS1 signaling. These results point to abnormal IGF1R signaling in the brain as a mediator of neurological sequelae in RA and provide support for the potentially reversible nature of hippocampal changes.

arthritis | IGF1 receptor | hippocampus | pain | MRI

Rheumatoid arthritis (RA) is an autoimmune disorder characterized by severe joint inflammation. If left untreated, RA leads to irreversible skeletal damage and progressive functional impairment. The central nervous system is not considered to be the primary target of the disease; however, neurological symptoms such as chronic pain, loss of motivation and depression, overwhelming fatigue, and memory and concentration difficulties are well documented and may be found in 13–42% of RA patients (1–3). Poorly controlled, they compound the health problems of RA patients and have negative consequences for family relations, working ability, and quality of life (4, 5). Symptoms of pain and depression often have similar damaging impact on patients' functional performance as the one caused by disease activity and structural joint damage (1, 2). An overall feeling of physical improvement because of a reduction in pain and fatigue is among the most valued outcomes for patients' experience of antirheumatic treatment (4, 6).

Most of the cognitive symptoms related to RA are often viewed as a consequence of functional disabilities, joint damage, and chronic pain. This view appears to be supported by findings from both electroencephalography and functional brain imaging that showed amplified responses to nociceptive stimuli in RA patients compared with controls (7, 8), and by structural changes, including somewhat smaller intracranial volumes and localized gray matter differences of subcortical structures (9, 10). Chronic inflammation with increased systemic levels of cytokines TNFα and IL-6 and high local cytokine production in the brain has recently emerged as a risk factor for cognitive impairment (11, 12). Treatment of RA patients with biological inhibitors of TNFα and IL-6 demonstrated the important role of these cytokines in disease perception (6, 13). Despite the documented enrichment of IL-1β, IL-6, and TNFα in the cerebrospinal fluid of RA patients (14–16), the understanding of molecular pathology behind neurological symptoms in RA patients remains incomplete.

Recent studies presented evidence of a connection between inflammation and compromised sensitivity to insulin and insulin-like growth factor 1 (IGF1). Epidemiological studies in RA point to systemic inflammation as an inducer of insulin resistance, a condition in which an increase in insulin release is needed to obtain

Significance

Aberrant insulin-like growth factor 1 receptor (IGF1R)/insulin receptor signaling in brain has recently been linked to neurodegeneration in diabetes mellitus and in Alzheimer's disease. In this study, we demonstrate that functional disability and pain in patients with rheumatoid arthritis (RA) and in experimental RA are associated with hippocampal inflammation and inhibition of IGF1R/insulin receptor substrate 1 (IRS1) signal, reproducing an IGF1/insulin-resistant state. This restricts formation of new neurons in the hippocampus, reduces hippocampal volume, and predisposes RA patients to develop neurological symptoms. Improving IRS1 function through down-regulation of IGF1R disinhibits neurogenesis and can potentially ameliorate neurological symptoms. This opens perspectives for drugs that revert IGF1/insulin resistance as an essential complement to the antirheumatic and antiinflammatory arsenal.

Author contributions: M. Pekna, M. Pekny, K.O., M.K., and M.I.B. designed research; K.M.E.A., C.W., L.J., L.L., M.C.E., S.T.S., A.S., and R.A.H. performed research; M. Pekna, K.O., and M.K. contributed new reagents/analytic tools; K.M.E.A., C.W., L.J., L.L., M.C.E., and R.A.H. analyzed data; and K.M.E.A., C.W., M. Pekna, R.A.H., and M.I.B. wrote the paper.

The authors declare no conflict of interest.

This article is a PNAS Direct Submission.

[1]K.M.E.A. and C.W. contributed equally to this work.

[2]To whom correspondence may be addressed. Email: karin.andersson@rheuma.gu.se or maria.bokarewa@rheuma.gu.se.

This article contains supporting information online at www.pnas.org/lookup/suppl/doi:10.1073/pnas.1810553115/-/DCSupplemental.

Published online December 3, 2018.

a quantitatively normal response. The prevalence of insulin resistance is as high as 51–58% in RA patients and correlates with systemic inflammation reflected by TNFα, IL-6, and C-reactive protein (17–19). Other features of deregulation in signaling through IGF1 receptor (IGF1R) are also present in RA. Although serum levels of IGF1 are low in RA patients (20, 21), IGF1R signaling is increased in leukocytes and synovial cells of RA patients (21, 22) conceivably due to activation of IGF1R by alternative ligands, for example, insulin and adipokines. High IGF1R expression in peripheral leukocytes of RA patients was associated with high serum levels of IL-6, erythrocyte sedimentation rate, and high expression of transcription factor NF-κB regulating production of proinflammatory cytokines in leukocytes (23).

In the brain, insulin receptors (IRs)/IGF1R exist predominantly as heterodimers and display substantially higher affinity toward IGF1 than insulin (24, 25). IGF1R is expressed in neural progenitor cells, mature pyramidal, and granule neurons during development of the hippocampus (HC) (26). IGF1R signaling is critical for neurogenesis as the loss of IGF1 or IGF2 leads to microcephaly, and IGF1R-deficient mice have smaller dentate gyrus (DG) and cornu ammoni (CA) (27). Brain tissue is sensitive to IGF1R stimulation, responding with brain enlargement to overexpression of IGF1 (26). In healthy adult HC, IGF1R modulates granule cell transition from neural progenitor cells to mature neurons in the DG. IGF1R is intimately engaged in directing the positioning of newly formed mature neurons within the DG_{sg} and in promoting synapse formation with pyramidal neurons in CA (CA_{sp}) and spineless dendrites in the molecular layer (DG_{mo}) (24, 25). After traumatic brain injury, IGF1R mediates neurotrophic and neuroregenerative signals that stimulate neuronal survival and differentiation in the DG_{sg}.

A direct connection between IR/IGF1R signaling and brain function has been proposed for the process of neurodegeneration in conjunction with neuropsychiatric symptoms in human studies and in mouse models of neurological disease including Alzheimer's disease (AD) and depression (28–31). Furthermore, type 2 diabetes, the canonical condition represented by insulin resistance, is associated with cognitive decline, brain hypometabolism, and regional atrophy (32–34). The underlying mechanism of altered insulin/IGF1 sensitivity is related to the common signaling path downstream of IR/IGF1R, to low levels of IR substrates (IRSs), and to the inhibitory serine phosphorylation (30, 35). Whether IGF1R signaling in the brain is subsequently affected by systemic inflammation in RA is not known, but ample evidence of a role for IGF1R in neurogenesis and neurological symptoms attracts attention.

In the present study, we address the association between IGF1/IGF1R signaling and neurological symptoms in RA. In RA mice, arthritis led to increased density of $IBA1^+$ microglia in the HC, which facilitated enrichment in the inhibitory pS^{612} IRS1 and impaired IGF1R signaling essential for neurogenesis. Blocking IGF1R alleviated arthritis, reduced pS^{612} IRS1, and improved neurogenesis. We show a connection between IGF1R expression in leukocytes of the peripheral blood and reduced physical activity in RA patients, which is further associated with smaller volume of the HC. Collectively, these findings point to IGF1/IGF1R signaling in the brain being an important mediator of neurological signs and symptoms in RA.

Results

Collagen-Induced Arthritis Causes Behavioral Changes in Mice. Immunization with collagen type II (CII) led to spontaneous development of arthritis (Fig. 1*A*). The CII-induced arthritis started on day 19 from digital areas of the paws and progressed gradually in severity engaging the tarsal, metatarsal, and talocrural joints of the hindpaws. The mean arthritis severity index increased to 17 (range, 7–30) by the end of the experiment (day 41; Fig. 1*A*). The progressive nature of arthritis was clearly seen from the increased number of swollen joints, from the gradual loss of body weight of the arthritic mice compared with the naive siblings (Fig. 1*B*), and from high serum levels of IL-6 (Fig. 1*C*). The damage in skeletal structures of the arthritic joints was verified by micro-computed tomography (Fig. 1*D*) and was represented by development of erosions on the articular surfaces of bones and significant loss in bone volume in the periarticular regions of the hindpaws. This chronic, progressive, and joint-damaging inflammatory process, referred to in the following as "RA mice," strongly resembled the phenotype of RA in humans.

The development of arthritis was accompanied by significant behavioral changes in RA mice. The naive mice displayed an active behavioral pattern with remarkable consistency between the records on days 2, 19, and 40. They spent 70% of the time in locomotion and rearing, while immobility and minor movements covered only 10% of their activities (Fig. 1*E*). RA mice were different (Fig. 1*E*). On day 2 after the immunization, the RA mice presented signs of hyperactivity with prolonged locomotion and reduced time in grooming and minor movements. On day 19, at early clinical signs of arthritis, the mice dramatically reduced locomotion and rearing, and substituted those activities with minor movements. At the stage of severe arthritis (day 40), the mice showed further reduction in locomotion and rearing, while immobility and minor movements were prolonged and covered on average 44% of the time (Fig. 1*E*). This reduction in locomotion and rearing correlated with the severity of arthritis, loss of body weight, and serum levels of IL-6 (Fig. 1*F*).

RA Mice Exhibit Signs of Inflammation in the HC. The behavioral changes that we observed in RA mice have recently been related to activation of spinal microglia and astrocytes (14, 15). In the present study, the distribution of microglia within the HC was investigated by staining of brain sections for the IBA1 protein. Furthermore, the microglia activation status was assessed by mRNA quantification of CD68 and IL-1β. The morphometric analysis revealed an increase in the overall density of $IBA1^+$ cells in the HC of RA mice [in cells/mm^2: 186.5 (114–275) vs. 113.3

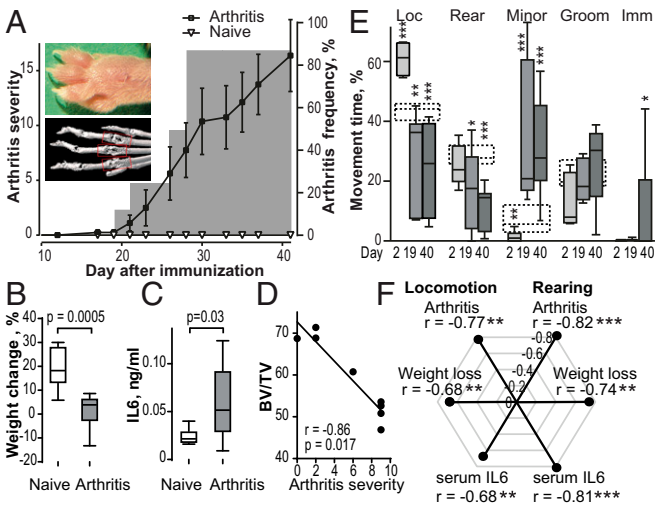

Fig. 1. Collagen-induced arthritis causes behavior changes in mice. (*A*) Subcutaneous immunization of DBA/1 mice with chicken CII resulted in spontaneous arthritis, which progressed in frequency and severity. *Insets* show clinical arthritis in the digital and metatarsal areas, and skeletal damage in a 3D micro-computed tomography image of the same areas. The red boxes indicate the areas of analysis. (*B*) The changes in body weight and (*C*) serum IL-6 levels in RA mice compared with naive siblings. (*D*) Spearman's correlation shows a gradual reduction in proportion of bone volume within tissue volume (BV/TV) with arthritis severity. (*E*) Behavioral pattern of RA mice was registered by filming and presented as time occupied in each activity (locomotion, rearing, minor movements, grooming, and immobility). The dotted boxes present median and interquartile range of the naive siblings filmed on the same occasion. (*F*) Spearman's correlations (rho values) of arthritis severity, body weight loss, and serum IL-6 levels with locomotion and rearing is shown. Boxplots present median, interquartile range, and full range. *P* values are calculated with the Mann–Whitney *U* test between RA mice (filled boxes) vs. naive, nonimmunized mice (open boxes). $*P < 0.05$; $**P < 0.01$; $***P < 0.001$.

(90–141); $P = 0.052$]. Specifically, IBA1$^+$ cells were enriched in the DG_{mo} (in cells/mm^2: 205.5 vs. 108.1; $P = 0.017$) and in the CA_{sp} (in cells/mm^2: 129.6 vs. 66.9; $P = 0.017$), primarily in the CA1 and CA3 fields (Fig. 2 *A* and *B*). Interestingly, IBA$^+$ microglia cells retained their ramified morphology with three or more processes, similar to those in naive mice. The higher density of IBA$^+$ cells in the RA HC was associated with significantly higher levels of the microglia activation marker CD68 and the inflammatory cytokine IL-1β mRNA (Fig. 2*C*), while the expression of proinflammatory chemokines CCL2 and CCL3 was not altered in the RA HC (Fig. 2*C*). The density of IBA1$^+$ cells in the DG_{mo} and CA_{sp} correlated with the loss of body weight ($r = 0.70$ and $r = 0.55$, respectively) and arthritis severity ($r = 0.67$ and $r = 0.56$, respectively) and mRNA CD68 in HC ($r = 0.63$ and $r = 0.57$, respectively), and also with inactive behavior in the RA mice including reduction of locomotion ($r = -0.95$ and $r = -0.48$, respectively) and increase in the minor movements ($r = 0.72$ and $r = 0.77$, respectively) (Fig. 2*D*).

Neurogenesis Is Compromised in the DG of RA Mice. Given that HC inflammation often has a negative neurotrophic effect, we next evaluated the morphology of the HC formation in the RA and naive mice.

We found that the total area of the HC was substantially smaller in RA compared with naive mice ($P = 0.015$; Fig. 3*A*). The difference was most pronounced in the DG. The DG_{sg}, where new neurons develop throughout the life span, was particularly affected in RA mice and the average thickness was reduced (in μm: 70.2 vs. 63.3; $P = 0.055$; Fig. 3*B*). The analysis of brain sections for doublecortin (DCX), a marker of neuroblasts and immature neurons, identified DCX$^+$ cells exclusively along the border of DG_{sg} (Fig. 3*H*). The median number of DCX$^+$ cells, normalized to the length of the DG_{sg} border, was 4.18 (2.50–9.56) cells/mm in RA mice vs. 8.14 (4.54–11.85 cells/mm) in naive mice ($P = 0.16$) (Fig. 3*C*). In addition, the mRNA levels of DCX and the proliferation marker Ki67 were significantly reduced in the HC of RA mice compared with naive mice (Fig. 3*L*). Importantly, the area of DG_{sg} was positively correlated to the density of DCX$^+$ cells ($r = 0.72$; $P = 0.0047$; Fig. 3*D*), pointing to a relationship between smaller DG and impaired neurogenesis in RA mice. There was an inverse correlation between low DCX mRNA with higher density of IBA1$^+$ cells in DG_{mo} (Fig. 2*D*) and mRNA levels of CD68 ($r = -0.70$; $P = 0.005$) and IL-1β ($r = -0.56$; $P = 0.005$) in HC.

To study potential impact of neural degeneration in the reduction of the HC volume in RA mice, we performed Fluoro-Jade C (FJC) staining. Whereas FJC$^+$ cells were clearly seen in the DG of mice after hypoxic–ischemic brain injury (*SI Appendix*, Fig. S1), no FJC$^+$ cells could be found in the HC of naive and RA mice. These findings support the notion that compromised neurogenesis rather than degeneration is the primary reason for smaller HC in RA mice.

RA Mice Show Aberrant IGF1R Signaling in the HC. The IGF1R is abundantly expressed by neurons in the HC and is considered to be essential for their morphology and function (24, 25). We hypothesized that suppressed signaling through the receptor might be responsible for the impaired neurogenesis and reduction in HC size that were observed in RA mice. First, we analyzed the expression of IGF1 on a systemic and local level, but found no change in either serum IGF1 [in ng/mL: 125 (64.6–367) vs. 91.1 (46.5–133); $P = 0.12$] or HC IGF1 mRNA levels (Fig. 3*L*) in RA mice.

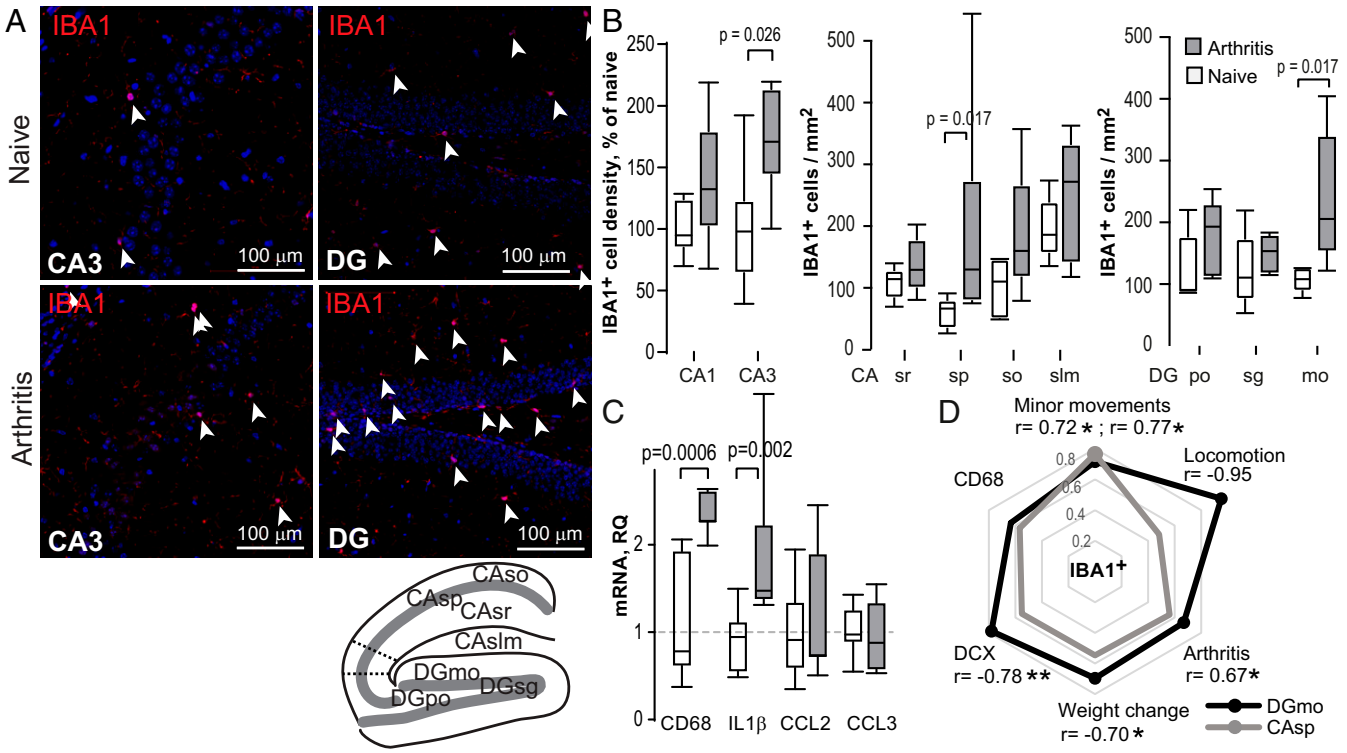

Fig. 2. Enrichment of IBA1$^+$ cells in the HC during arthritis. (*A*) The localization pattern of IBA1$^+$ cells (red, arrowheads) in DG and CA area of RA mice and naive controls. The area of the HC was determined from nuclei staining (blue). (*B*) The density of IBA1$^+$ cells within CA areas and layers of DG. (*C*) Gene transcription analysis in the HC tissue of naive and arthritic mice done with RT-PCR. (*D*) Spider chart of Spearman's correlations (rho values) between the density of IBA1$^+$ cells within DG_{mo} (black line) and CA_{sp} (gray line). Boxplots indicate median, interquartile range, and full range. *P* values are calculated with the Mann–Whitney *U* test between RA mice (filled boxes) vs. naive, nonimmunized mice (open boxes). $*P < 0.05$; $**P < 0.01$; $***P < 0.001$. CA, cornu ammonis; DG, dentate gyrus; mo, molecular layer; po, polymorph layer; sg, subgranular layer; slm, stratum lacunosum-moleculare; slu, stratum lucidum; so, stratum oriencs; sp, pyramidal layer; sr, stratum radiatum.

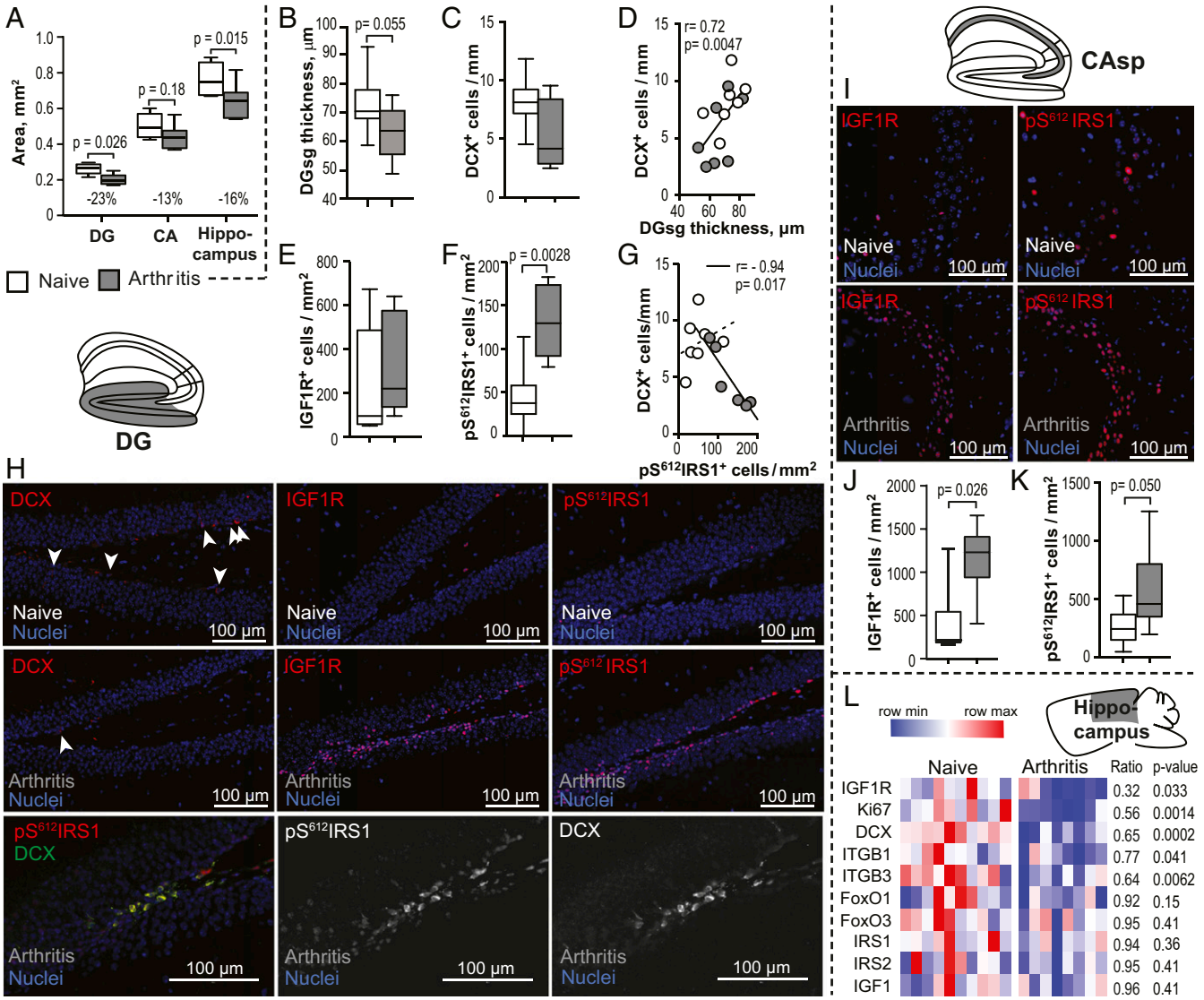

Fig. 3. Resistance to IGF1R signaling inhibits neurogenesis in HC during arthritis. Morphometric analysis of the HC of arthritic and naive mice (*A–K*). (*A*) The area of DG, CA, and total HC was measured from nuclei staining (blue) of 4-µm tissue sections. (*B*) The change in average thickness of DG_{sg}. (*C*) Density of DCX^+ cells in DG_{sg} layer as normalized to the length. (*D*) Spearman's correlation indicates a reduction in the thickness of DG_{sg} with lower number of DCX^+ cells. (*E*) The density of $IGF1R^+$ cells and (*F*) $pS^{612}IRS1^+$ cells in DG. (*G*) The Spearman correlation between the density of DCX^+ and $pS^{612}IRS1^+$ cells in DG. (*H*) Representative images of the HC staining show distribution of DCX^+ (indicated by arrowheads), $IGF1R^+$, and $pS^{612}IRS1^+$ cells in DG of naive (*Upper* row) and arthritis mice (*Middle* row). *Bottom* shows colocalization (yellow staining) of $pS^{612}IRS1$ and DCX in DG. (*I*) Representative image of the CA_{sp} subfield shows enrichment of $IGF1R^+$ and $pS^{612}IRS1^+$ cells in arthritis compared with naive mice. (*J* and *K*) The density of $IGF1R^+$ cells (*J*) and $pS^{612}IRS1^+$ cells (*K*) within CA_{sp} layer. (*L*) Heatmap shows transcriptional analysis of genes involved in neurogenesis and IGF1 signaling in the HC tissue of naive and arthritis mice, done by RT-PCR. Box plots present median, interquartile range, and full range. *P* values are calculated with the Mann–Whitney *U* test between RA mice (filled boxes) vs. naive, nonimmunized mice (open boxes). CA, cornu ammonis; DCX, doublecortin; DG, dentate gyrus; sg, subgranular layer; sp, pyramidal layer.

Next, we investigated the distribution of IGF1R in the HC. Surprisingly, we found higher density of $IGF1R^+$ cells in RA mice. The density of $IGF1R^+$ cells was highest in areas accumulating neuronal cell bodies, that is, the CA_{sp} and DG_{sg} layers. RA mice displayed a 5.5-fold increase in $IGF1R^+$ cell density within the CA_{sp} (in cells/mm^2: 1,204 vs. 218; $P = 0.026$; Fig. 3*J*) and no increase in the DG_{sg} (in cells/mm^2: 173 vs. 93; $P = 0.35$; Fig. 3*E*). The RA mice had lower IGF1R mRNA levels ($P = 0.033$; Fig. 3*L*) and its coreceptors integrin subunits β_3 (Itgb3) ($P = 0.0062$) and β_1 (Itgb1) ($P = 0.041$), which are required for neural stem cell development and positioning (36). Still, the mRNA levels of stem cell protective system of transcription factors FoxO1 and FoxO3, controlled by the IGF1R signaling, was not altered in the HC of RA mice (Fig. 3*L*).

Asking whether RA mice with augmented neurogenesis were becoming unresponsive to IGF1 signaling, we analyzed the IRSs (IRS1/2), downstream signaling adapter proteins of IGF1R. There was no difference in mRNA expression of IRS1 or IRS2 in the HC of RA mice and naive siblings (Fig. 3*L*). Next, we analyzed the activation status of the IRS1 protein by staining for the inhibitory serine-612 (S^{612}) phosphorylation. We observed that the density of $pS^{612}IRS1^+$ cells was significantly higher in the HC in RA mice ($P = 0.0048$). Importantly, $pS^{612}IRS1^+$ cells were localized along the border of the DG_{sg} and in the CA_{sp} (Fig. 3 *H* and *I*). The density of $pS^{612}IRS1^+$ cells was significantly higher in the DG_{sg} (in cells/mm^2: 129.5 vs. 37.6; $P = 0.0028$; Fig. 3*F*) and in the CA_{sp} (in cells/mm^2: 460 vs. 246; $P = 0.049$; Fig. 3*K*) of RA mice compared with naive. This pointed to an acquired reduction in responsiveness to IGF1/IGF1R signaling in RA mice. In RA mice, but not in naive mice, we observed a strong inverse correlation between the density of $pS^{612}IRS1^+$ in the DG_{sg} and the

number of DCX$^+$ neuroblasts in the same area ($r = -0.94$; $P = 0.0017$; Fig. 3*G*). Costaining experiments revealed colocalization of pS^{612}IRS1$^+$ and DCX$^+$ cells in RA and naive mice (Fig. 3*H*). A correlation was observed between DCX$^+$ and IGF1R$^+$ cells in the DG$_{sg}$ of RA mice ($r = -0.93$; $P = 0.008$; $n = 7$), but not in the naive mice ($r = -0.08$; $n = 6$). Taken together, these data support the conclusion that RA leads to inhibitory phosphorylation of S^{612} in IRS1 in the HC with negative consequences for its size.

Inhibiting IGF1R Improves Neurogenesis in RA Mice. To further pinpoint the role of the increased IGF1R expression in inflammation and declining neurogenesis following RA development, we inhibited IGF1R by treating the RA mice with short hairpin RNA (shRNA)-producing construct (shIGF1R) starting from the first sign of arthritis on day 19 (Fig. 4*A*). Clinically, the inhibition of IGF1R delayed the onset and alleviated the severity of arthritis in its early stages. Systemic effects of the treatment were seen in a decreased number of IGF1R$^+$ MHCII$^+$ cells and IRS1 expression in the spleens, and significantly increased serum levels of IGF1 (Fig. 4 *B* and *C*). However, no change in density of IGF1R$^+$ cells or IGF1R mRNA levels (Fig. 4*L*) was seen in the HC of shIGF1R-treated mice.

In the HC of shIGF1R-treated RA mice, significantly fewer IBA1$^+$ cells were found, indicating reduced inflammation. This reduction was clearly seen in the DG$_{mo}$ area (in cells/mm^2: 16 vs. 30; $P = 0.023$; Fig. 4*D*), in the stratum radiatum CA$_{sr}$ (in cells/mm^2: 12 vs. 95; $P = 0.016$) and in the CA$_{sp}$ (in cells/mm^2: 33 vs. 150; $P = 0.023$; Fig. 4*E*). Furthermore, the shIGF1R treatment significantly reduced also the density of pS^{612}IRS1$^+$ cells in the DG (Fig. 4*F*), which, in combination with higher serum IGF1, predisposed to improvement of IGF1R signaling.

To evaluate the impact of shIGF1R treatment in different stages of neuronal development, the brain tissue sections were stained for GFAP, a marker of an early stage, and DCX, a

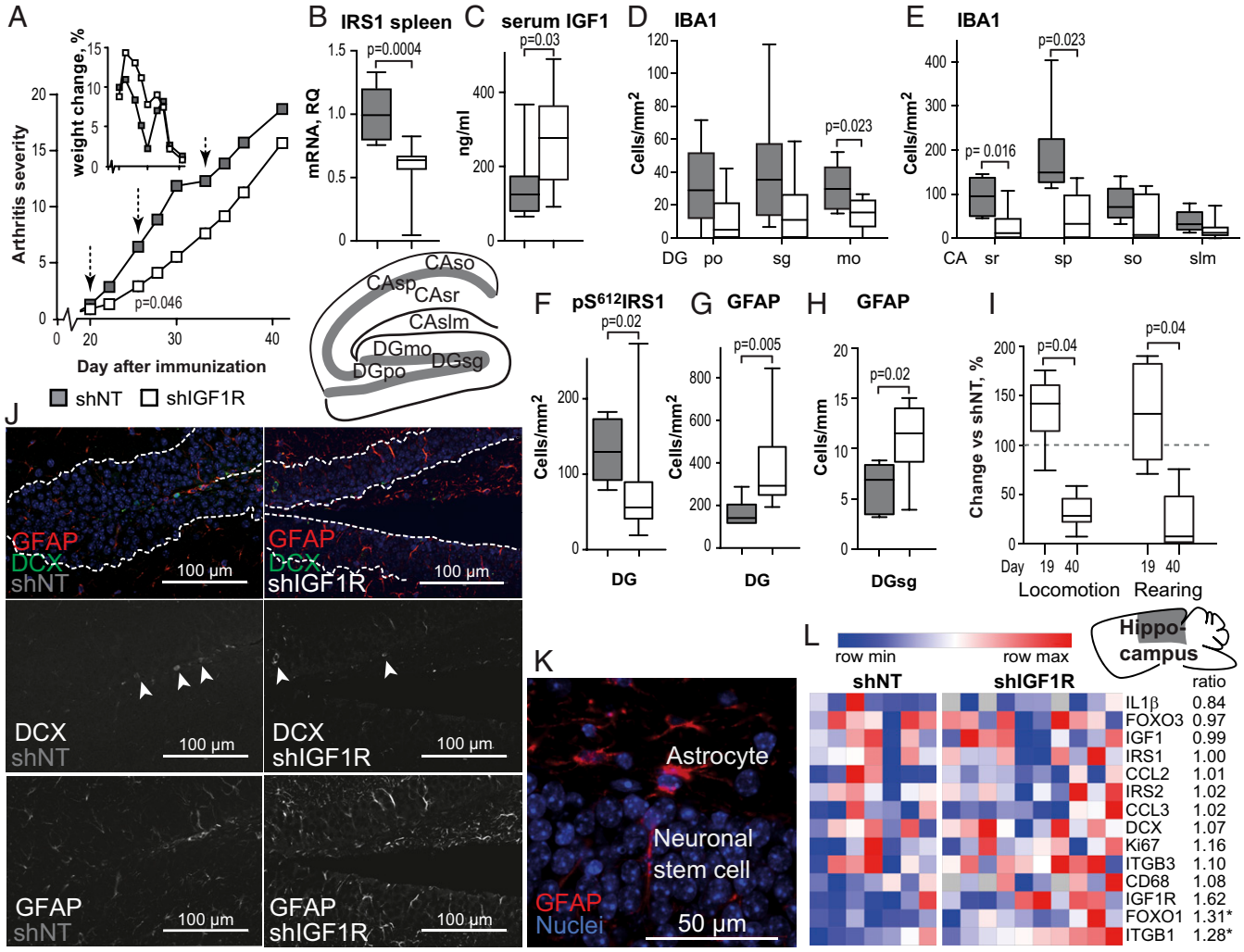

Fig. 4. Inhibition of IGF1R alleviates collagen-induced arthritis and supports early neurogenesis. (*A*) IGF1R was inhibited with shRNA (shIGF1R, empty symbols) provided intraperitoneally on days 19, 26, and 33 (indicated by arrows). The control group received nontargeting scrambled RNA (shNT) (filled symbols). Inhibition of IGF1R alleviated severity of arthritis and weight loss (*Inset*) in mice. Inhibition of IGF1R (*B*) reduced IRS1 mRNA in spleen, (*C*) increased serum levels of IGF1, and reduced the cell density of IBA1$^+$ cells in DG (*D*) and CA (*E*). (*F*) Change in density of pS^{612}IRS1$^+$ cells in DG. (*G* and *H*) Change in density of GFAP$^+$ cells in total DG and in DG$_{sg}$. (*I*) Reduction in behavioral activity of shIGF1R-treated mice. (*J*) The brain sections show costaining for GFAP and DCX in DG. The dotted line indicates the borders of DG$_{sg}$. The arrowheads indicate positive cells. (*K*) Different morphology of GFAP$^+$ cells in DG$_{sg}$, distinct from vertical-oriented neuronal stem cells from astrocytes. (*L*) Heatmap shows transcriptional analysis of genes involved in neurogenesis and IGF1R signaling in the hippocampal tissue of shIGF1R-treated and shNT-treated RA mice, done by RT-PCR. Boxplots present median, interquartile range, and full range. *P* values are calculated with the Mann–Whitney *U* test, between shIGF1R-treated mice (open boxes) vs. control, shNT (filled boxes). *$P < 0.05$. CA, cornu ammonis; DG, dentate gyrus; GFAP, glial fibrillary acidic protein; mo, molecular layer; po, polymorph layer; sg, subgranular layer; slm, stratum lacunosum-moleculare; slu, stratum lucidum; so, stratum oriencs; sp, pyramidal layer; sr, stratum radiatum.

marker of a later stage in this process. GFAP$^+$ neural stem cells could be distinguished from astrocytes by their location and morphology (Fig. 4*K*). We observed that GFAP$^+$ cells in the DG_{sg} also coexpressed DCX to some degree, but there were also cells expressing only one of the markers (Fig. 4*J*). Practical outcome of the reduced density of IBA1$^+$ cells and suppressed inflammation in the HC was associated with significant increase of the radially oriented GFAP$^+$ cells lining the border of the DG_{sg}, but also an increase in the density of GFAP$^+$ astrocytes in DG ($P = 0.022$ and $P = 0.005$, respectively; Fig. 4 *G* and *H*). In concordance with the larger pool of neural stem cells, we found higher levels of FoxO1 ($P = 0.025$) and Itgb1 ($P = 0.0016$) mRNA, indicating the early differentiation phase in the HC of shIGF1R-treated RA mice (Fig. 4*L*). However, shIGF1R treatment did not change the levels of DCX and Ki67 mRNA. This incomplete reactivation of neurogenesis potentially explains why the thickness of the DG_{sg} was still significantly decreased in shIGF1R-treated RA mice compared with the naive siblings, and was associated with further reduction of the time in locomotion and rearing (Fig. 4*I*). Given that mRNA level of CD68 and IL-1β in the HC remained similar between the shIGF1R-treated and shNT-treated RA mice (Fig. 4*L*), this aggravation of inactivity is unlikely to be attributed to arthritis or to local inflammation in the brain.

Smaller Volume of the HC in RA Patients Is Associated with Higher Functional Disability and Aberrant IGF1R Signaling. To study whether neuropsychological symptoms in RA patients are linked with HC size, we performed MR image-based HC volumetry in 15 randomly

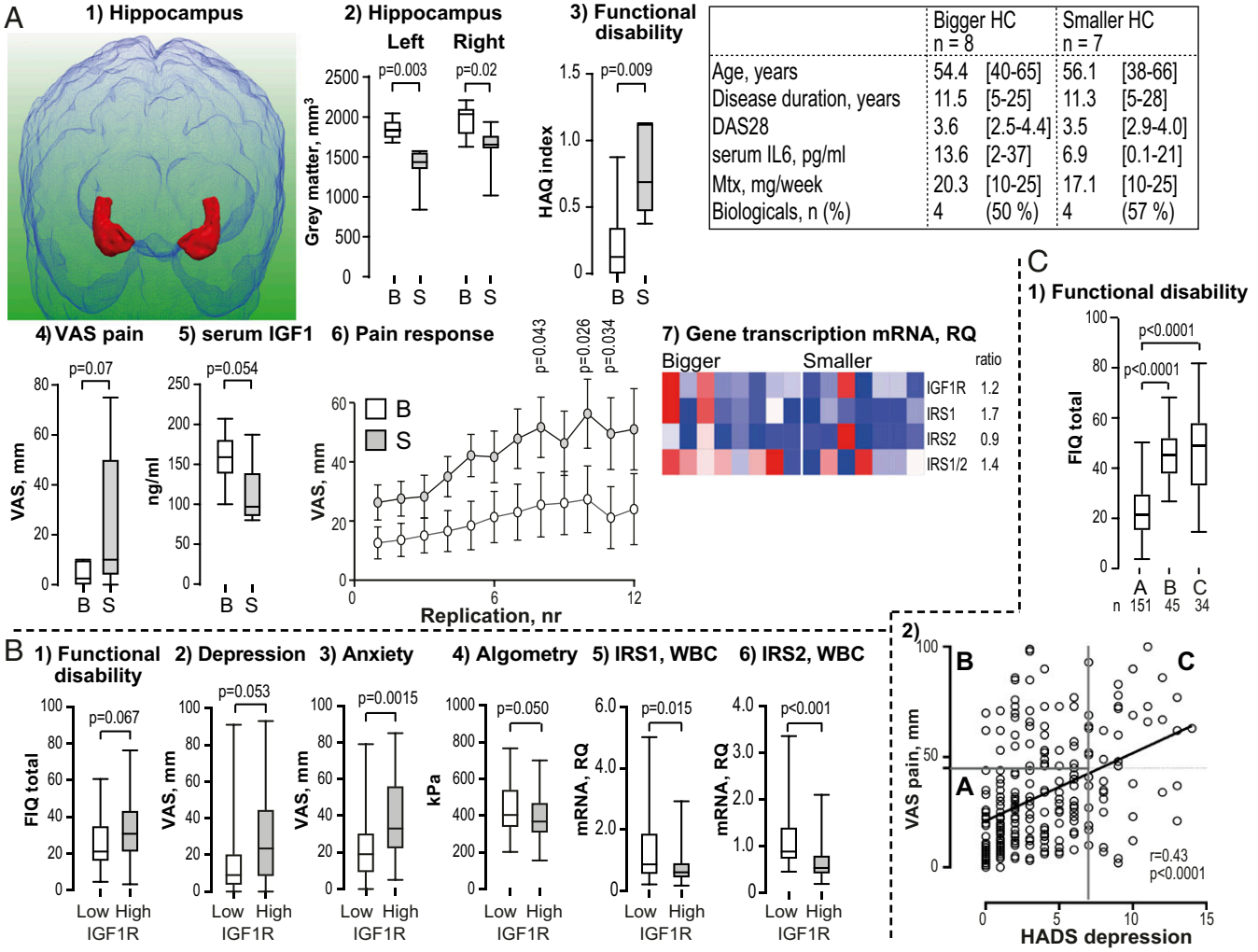

	Bigger HC n = 8		Smaller HC n = 7	
Age, years	54.4	[40-65]	56.1	[38-66]
Disease duration, years	11.5	[5-25]	11.3	[5-28]
DAS28	3.6	[2.5-4.4]	3.5	[2.9-4.0]
serum IL6, pg/ml	13.6	[2-37]	6.9	[0.1-21]
Mtx, mg/week	20.3	[10-25]	17.1	[10-25]
Biologicals, n (%)	4	(50 %)	4	(57 %)

Fig. 5. The volume of HC in patients with RA correlates with IGF1R signaling and functional disability. (*A*, *1*) A 3D surface rendering of the HC in the postero-anterior view is shown. Anatomical segmentation of MR images in 15 female RA patients separated the group with the HC volume above the median (bigger HC, $n = 8$) and below the median (smaller HC, $n = 7$). Clinical characteristics of the patients are shown in the table. Boxplots show (*A*, *2*) gray matter volumes in the left and right HC gyrus, in absolute numbers normalized by intracranial volume; (*A*, *3*) difference in functional disability, (*A*, *4*) pain perception, and (*A*, *5*) serum levels of IGF1 in RA patients with different HC volume. (*A*, *6*) Change in pain perception recorded with replication of pressure applied on meta-carpophalangeal joint II. (*A*, *7*) Heatmap shows transcriptional analysis of genes involved in IGF1R signaling in WBC, done by RT-PCR. (*B*) Expression of IGF1R in WBC was measured in 84 randomly selected female RA patients by RT-PCR, and the groups with IGF1R above and below the lower tertile for the group were compared. Boxplot shows (*B*, *1*) functional disability assessed by the Fibromyalgia Impact Questionnaire (FIQ); perception of (*B*, *2*) depression and (*B*, *3*) anxiety; (*B*, *4*) pain threshold measured by algometry; and (*B*, *5*) levels of IRS1 mRNA and (*B*, *6*) IRS2 mRNA in WBCs measured by RT-PCR. (*C*) Functional disability (*C*, *1*) was assessed by FIQ and compared in 230 RA patients (female, 171; male, 59) within the groups of (*C*, *2*) nondepressed (group A), nondepressed with severe pain (group B; VAS > 45 mm, HADS ≤ 7) and with depression (group C; HADS ≥ 8). Box plots demonstrate median, interquartile range, and full range. *P* values are estimated with the Mann–Whitney *U* test or the Kruskal–Wallis nonparametric ANOVA. B, bigger; FIQ, Fibromyalgia Impact Questionnaire; HADS, Hospital Anxiety and Depression Scale; HAQ, Health Assessment Questionnaire; HC, hippocampus; MR, magnetic resonance; RA, rheumatoid arthritis; S, smaller; VAS, visual analog scale; WBC, white blood cell.

selected female RA patients (Fig. 5*A*). All of the patients reported to be right-handed, which justified ranking the patients by absolute gray matter volume of the left HC gyrus and separating at the median value into two groups (Fig. 5 *A*, 1 and 2). The difference in the HC volume was consistent in both hemispheres. The groups were comparable in age, RA duration, and disease activity as measured by Disease Activity Score by Assessment of 28 Joints (DAS28). However, the patients with a relatively small HC volume reported more severe functional disability reflected by Health Assessment Questionnaire (HAQ) score (Fig. 5 *A*, *3*). Additionally, we found that patients with small HC recorded a numerically higher general pain perception on visual analog scale [in mm: 45.6 (11–89) vs. 21.7 (2–57); $P = 0.068$] during the week before the MR investigation, and they differed significantly in functional pain response during replicated stimulation by pressure (Fig. 5 *A*, *4* and *6*). We also found that smaller HC volume was associated with somewhat lower serum IGF1 (in ng/mL: 97 vs. 159; $P = 0.054$; Fig. 5 *A*, *5*) and lower IGF1R and IRS1 mRNA in blood leukocytes (Fig. 5 *A*, *7*), which supported the notion of disturbances in IGF1R signaling of these patients.

To determine whether IGF1R expression is connected with neuropsychological symptoms in RA, we assessed the physical functioning of 84 randomly selected female patients with established RA (Fig. 5*B*). Patients with high IGF1R mRNA levels (above the lower tertile) in leukocytes reported a tendency to higher functional disability with total Fibromyalgia Impact Questionnaire (FIQ) (Fig. 5 *B*, *1*) and higher perception of depression and anxiety (Fig. 5 *B*, *2* and *3*). Additionally, the measures of pain tolerance by algometry indicated lower thresholds in RA patients with high IGF1R (Fig. 5 *B*, *4*). These differences were associated with lower expression of IRS1 and IRS2 (Fig. 5 *B*, *5* and *6*) and low serum IGF1 [in ng/mL: 167 (51–319) vs. 128 (71–345); $P = 0.006$], but are not likely due to higher disease activity, since the number of swollen and tender joints was similar.

To further confirm the link between physical functioning and neuropsychological symptoms, we analyzed a group of 230 RA patients (Fig. 5*C* and Table 1). Data were collected using established self-reporting tools, specifically the Fibromyalgia Inactivity Questionnaire, the general pain perception by visual analog scale (VAS), and the Hospital Anxiety and Depression Scale (HADS). Physical functioning in RA patients showed a gradual decrease from the nondepressed patients, via the patient group with incongruous data (VAS pain > 45 mm, but HADS ≤ 7; $n = 41$; $P < 0.0001$), to the patients with depression confirmed by HADS (HADS ≥ 8; $n = 36$; $P < 0.0001$).

These clinical observations in RA patients present a direct link to the results obtained in RA mice, where remote inflammation in the brain of mice with arthritis was associated with a reduction in physical activity.

Discussion

In the present study, we demonstrate that pain-inflicted functional disability in clinical and experimental RA is associated with aberrant IGF1R signaling caused by resistance to IGF1 stimulation, inadequate maintenance of HC neurons, and reduced HC volume.

First, we showed that experimental RA leads to neuroinflammation in the HC manifested as increased density of $IBA1^+$ cells accompanied by high levels of proinflammatory cytokine IL-6 in serum and in situ production of IL-1β in the brain and in the HC. We also observed increased S^{612} phosphorylation of IRS1 (pS^{612}IRS1), marking IGF1/insulin resistance in the HC. In RA mice, the increased density of $pS^{612}IRS1^+$ cells was prominent in the DG_{sp}, $CA1_{sp}$, and $CA3_{sp}$ layers, and inhibited signal transduction initiated by IGF1R. This was associated with reduced DCX mRNA levels and number of DCX^+ developing neurons, and ultimately led to smaller tissue volume of the HC. In the absence of obvious signs of neurodegeneration and considering the importance of IGF1 signaling for normal development of neurons in the DG_{sg}, it is perhaps not surprising that the aberrant IGF1R signaling in the HC of RA mice was accompanied by a reduction in the number of DCX^+ cells and reduced thickness of the DG_{sg}. Similar molecular hallmarks of IGF1/insulin resistance have been identified in the HC of patients with AD, which is associated with atrophy of the HC and cognitive decline of those patients (28–30). This points toward pathogenetic commonalities between RA and AD and adds fuel to the unresolved discussion about causal links between these diseases (37).

Microglia have previously been identified as an essential early player in the neuroinflammatory cascade that may lead to neuronal cell loss (38). In fact, systemic and intracerebral increase in cytokines and other signal molecules is considered to be a clinically relevant indicator of cognitive impairment (39, 40) and is suggested to precede development of AD (41, 42). These proinflammatory cytokines, including IL-1β, IL-6, and TNFα are central to the pathogenesis of RA. In our study, arthritis was associated with high IL-6 in serum and in situ production of IL-1β in the brain, which provoked neuroinflammation by increased density of $IBA1^+$ inflammatory cells in the HC. Importantly, production of IL-6 and IL-1β may be viewed as a direct cause of inhibitory pS^{612}IRS1 (43, 44), which restricts signaling and compromises sensitivity of the brain cells to insulin and IGF1. Importantly, we show that a connection between smaller HC volume and disturbed IGF1R signaling also exists in RA patients. These morphological changes in the HC were associated with significant alterations in behavior and decline of physical functioning in patients with RA and in RA mice.

Peripheral insulin/IGF1 resistance, defined by higher serum insulin levels being required for adequate glucose metabolism, is a frequent finding in RA patients (18, 19). Importantly, peripheral insulin resistance is associated with low glucose metabolism in the temporal lobe (45). It has also been reported as a sensitive predictor of cognitive decline in middle-aged nondiabetic patients with progressive deterioration in verbal fluency and with reduced performance in immediate and delayed memory tests (46–48). Our clinical data provide important insights into the connection between IGF1R signaling, HC volume, and physical activity. In a pilot study using structural MR image analysis in female RA patients, we found an association between smaller volume of HC and low serum levels of IGF1 and imbalance of IGF1R and IRS1 mRNA levels in leukocytes. Since RA mice showed smaller HC and less active behavior, we sought to determine whether there was a link between smaller HC volume and functional disability in RA patients. Indeed, we found that smaller HC volume was associated with higher HAQ disability scores and with stronger pain response to pressure. In further support of such a link is the finding that RA patients with high IGF1R in WBCs had a decreased pain threshold and augmented perception of pain, anxiety, and depression. To our knowledge, the link between imbalance in IGF1R signaling and HC volume in clinical RA has not been described previously.

The present results are concordant with recent observations in older adults showing that physical activity increases HC volume

Table 1. Clinical characteristics of patients with RA

	RA cohort	IGF1R WBC	MRI study
Characteristics	*n* = 230	*n* = 84	*n* = 15
Females, *n* (%)	171 (74%)	84 (100%)	15 (100%)
Age, y	52 [21–69]	54 [21–71]	55 [38–66]
RA duration, y	11 [1–49]	9 [1–32]	11 [5–28]
DAS28	3.1 [0.7–6.6]	3.3 [1.0–6.6]	3.6 [2.5–4.4]
Serum IL-6, pg/mL	8.3 [0–176]	8.4 [0–73.3]	10.7 [0–37.5]
MTX, *n* (%)	203 (88%)	75 (89%)	15 (100%)
Dose, mg/wk	18 [5–25]	18 [5–25]	19 [10–25]
Biologics, *n* (%)	84 (37%)	34 (40%)	8 (53%)

Absolute values are presented as mean [range]. DAS28, Disease Activity Score by Assessment of 28 Joints; IGF1R, insulin-like growth factor 1 receptor; MRI, magnetic resonance imaging; MTX, methotrexate; RA, rheumatoid arthritis; WBC, white blood cell.

and improves cognition (49, 50). In an experimental context, physical exercise increased IGF1 levels, which contributed to survival of new neurons in the DG (51) and increased HC volume (52). Voluntary wheel running and enriched environments in the home cage blunted proinflammatory HC response by increasing expression of the antiinflammatory cytokines IL-1ra and CX3CL1 (53). The specific mechanism underlying the RA-induced behavioral changes in RA mice is currently unclear; however, CA pyramidal neurons are known to be involved in the control of locomotive activity (54). The changes in IGF1R expression and signaling observed in the CA area of RA mice present a potential explanation that warrants further investigation. Taken together, these results suggest that inactivity of RA patients may aggravate HC malfunction, which in turn further reduces physical activity, leading into a downward spiral.

Today, it remains unclear whether the RA-related changes observed in the HC are reversible or whether they may be efficiently prevented by timely initiation of IGF1/insulin sensitization measures in RA patients. Our findings that the inhibition of IGF1R expression by shIGF1R reduced the numbers of pS^{612} IRS1 cells and increased the pool of neural stem cells provide further support for the critical role of IGF1R signaling as a mediator of neurological sequelae of RA and for the potentially reversible nature of HC changes. Interestingly, several widely used antidiabetic drugs have antiinflammatory properties. Biguanide metformin, which increases the effectiveness of insulin through activation of adenosine monophosphate-activated protein kinase (AMPK), has recently been attributed antiinflammatory and antiarthritis effects (55). Glitazones, a different class of antidiabetic drugs increasing sensitivity to insulin by targeting peroxisome proliferator-activated receptors, decreased disease activity in nondiabetic RA patients (56, 57). Neuroprotective properties of antidiabetic drugs are about to be recognized. Activation of AMPK with metformin and supplementation with insulin ameliorated Alzheimer's-like pathology in mice (58, 59). Both metformin (60, 61) and glitazones (62) had favorable effect on pain. These reports support the notion of insulin sensitivity as a neuroprotective factor. Further investigation in experimental and clinical settings is warranted to follow up on these emerging leads.

This study puts aberrant IGF1R/IRS signaling in RA in a clinical perspective and shows its consequence for the structural and functional correlates in the brain. We present experimental evidence for a connection between RA-induced inflammation in the HC, increase in the density of cells with inhibitory serine phosphorylated IRS1 in the CA and DG subfields of the HC, followed by a reduction in neurogenesis and HC volume. These morphological changes may explain neurological symptoms of pain, depression, and cognitive deficits in RA patients and place RA in a row with common neurodegenerative diseases. Our findings open perspectives for a drug target in RA, as well as therapeutic repurposing of existing drugs to improve insulin sensitivity as a complementary treatment strategy in chronic inflammatory disorders.

Materials and Methods

Patients. The study cohort comprised 230 patients with RA who attended the Rheumatology Clinics at the Sahlgrenska University Hospital, Gothenburg, or the Rheumatology Unit at Uddevalla Hospital. The clinical characteristics of RA patients at enrollment are shown in Table 1. Based on clinical evaluation of swelling and tenderness in 28 joints and erythrocyte sedimentation rate, the disease activity score (DAS28) was calculated. The study was performed in accordance with the Declaration of Helsinki. The Ethical Committee at Sahlgrenska University Hospital approved the study (659-11; amendment T038-12 for MRI). Written and verbal information explaining the nature and possible consequences of the study was given to all patients, and written consent was obtained from all participants. The trial is registered at ClinicalTrials.gov with ID NCT03449589.

VASs, graded after a 100-mm scale, were used to record perception of pain, fatigue, and depression. Higher scores indicate more pain, fatigue, or depression.

Pain Assessment. All pain assessments were performed at a single visit and during morning hours. The patients were instructed to omit any nonsteroidal antiinflammatory drug use 18 h before the examination. Each patient recorded pain intensity during the preceding week on a VAS. To estimate pain distribution, a tender-point (TP) examination was performed by manually applying 40 N of force to 18 standard TPs used for the diagnosis of fibromyalgia (63). The total number and localization of TPs was recorded. Pain threshold was measured in kilopascals by using an electronic hand-held algometer (Somedic AB). In this study, the algometer was placed bilaterally on the nail of the thumb and on the second metatarsophalangeal joint, giving a total of four measurements. Functional pressure pain response in the MRI study was examined by compression of the left metacarpophalangeal joint with 40 N of force. Each stimulation block consisted of 10–12 stimulations for 10 s with 15-s interstimulus interval. During the interstimulus interval, the pain intensity was recorded on a VAS.

Physical functioning was calculated based on the FIQ, which consists of 11 items of simple daily activities (64). Restrictions in performing the activities during the week preceding the study are graded on a four-point scale as "not at all" (0 point), "sometimes" (one point), "often" (two points), and "always" (three points) and summarized. RA-related functional disability to perform everyday activities was assessed using a Swedish version of the Stanford Health Assessment Questionnaire (HAQ) (65). HAQ is a 20-item self-reporting tool to measure the ability to perform common basic activities such as dressing, eating, hygiene, shopping, and traveling, in which scores range from 0 to 3.

MR Evaluation of Brain Morphology. A total of 15 female patients was recruited from the RA cohort presented above (Table 1). To avoid unspecific group difference effects, the study included only females. At the time of the study, all patients were treated with methotrexate (MTX). Eight patients additionally received TNF inhibitors (infliximab, 4; adalimumab, 1; golimumab, 1; etanercept, 2). Two patients were treated with oral corticosteroids. All patients reported that they were right-handed.

MR Data Acquisition and Processing. Anatomical MR images of head were acquired using a 3-tesla scanner with a 32-channel SENSE head coil (Philips Gyroscan Achieva 3T; Philips Healthcare). Patients' heads were firmly supported with cushions to minimize movements. T1-weighted images were acquired with the following parameters: flip angle, 8°; echo time, 4.0 ms; repetition time, 8.4 ms; SENSE factor, 2.7; turbo field echo factor, 240, at a resolution of $1 \times 1 \times 1$ mm^3. Images were preprocessed with field inhomogeneity correction [N4ITK (66)] and brain extraction [pincram (67)] software. The MR images were blinded at acquisition. Automatic anatomical segmentation was performed using multiatlas propagation with enhanced registration (MAPER) (68) and the 2017 version of the "Hammers_mith" atlas database (95 regions; ref. 69). We limited the analysis to volumetry of the right and left HC regions.

Blood Sampling and Storage. Blood samples were obtained from the cubital vein and centrifuged at $800 \times g$ for 15 min; serum was aliquoted and stored frozen at –70 °C until use.

Collagen-Induced Arthritis. Male DBA/1 mice (8 wk old; Taconic Europe) were immunized s.c. with chicken CII (100 mg/mouse; Sigma-Aldrich) emulsified in an equal volume of complete (day 0) and incomplete (day 21) Freund's adjuvant as described previously (70). Experiments were terminated on day 41. All mice were housed at the animal facility at Guldhedsgatan 10A (Gothenburg, Sweden) under standard conditions of temperature and light, and fed laboratory chow and water ad libitum. The guidelines for the care and use of laboratory animals were strictly followed. The experiments were approved by the animal ethical board at the University of Gothenburg (permits 126-2012 and 272-2010).

Inhibition of IGF1R in Vivo. Lentiviral particles, MISSION TRCN0000023490 and TRCN0000023493 (Sigma-Aldrich), encoding shRNA targeting IGF1R (shIGF1R), or nontargeting shRNA controls, shNT (SHC002H; Sigma-Aldrich), were injected intraperitoneally (10^6 to 10^7 particles in 100 μL per mouse) on days 19, 26, and 33. The optimal dose and delivery frequency was set in cultures of PMA-stimulated splenocytes and in a pilot in vivo experiment (23). Toxicity of shRNA particles was tested by i.p. injection with 10^8 shNT particles in 100 μL and compared with vehicle (71). No signs of pain at injection site, inflammation, or change in total body or spleen weight were observed.

Evaluation of Arthritis. The paws were examined for swelling and redness in the digits, tarso-metatarsals, and ankles of the hindpaws (three regions), and in the digits and carpo-metacarpals of the forepaws (two regions) every other day by an observer blinded to the intervention protocol. Severity of arthritis was scored from 0 (no inflammation) to 3 individually for each of 10 paw regions. The arthritis index was constructed by adding the scores for each mouse (highest score, 30).

Micro-Computed Tomography. The left hindpaw of each mouse was scanned with a micro-CT (SkyScan 1176; Bruker) at a resolution of $9 \times 9 \times 9$ μm, as described (71). The projection images were reconstructed into 3D images using NRecon software (version 1.5.1; Bruker) and analyzed with CTAn (version 1.7; Bruker). The analysis of bone microarchitecture was performed within the intraarticular region of the metatarso-phalangeal III bone. The region of interest was set to 2.7 mm spanning over the joint. Measures of bone volume (BV) and tissue volume (TV) within each 3D region of interest were obtained.

Behavioral Tests. Behavioral analysis was performed on days 2, 19, and 40 after the CII immunization by filming during the period of 10 min, as described (72). A control group of naive siblings was filmed in parallel with RA mice on every occasion. The video records were analyzed using specially designed software, and the total record time was split into periods occupied by each activity: immobility (standing, sitting, or lying without movements), minor movements (standing, sitting, or lying at place changing position of head and paws), locomotion (walking or running around the cage), grooming (licking or rubbing parts of the body), and rearing (standing on hindpaws with front part of the body raised from the floor) (72).

Gene Expression Analysis. In patients, mRNA was purified from peripheral blood collected into PAXgene Blood RNA tubes (PreAnalytiX) as described (23). In mice, the tissue containing HC was excised from the right hemisphere and stored in Allprotect Tissue Reagent (Qiagen) in −20 °C. RNA was isolated with RNeasy Plus Universal Kit (Qiagen). Concentration and quality of the RNA were evaluated with a NanoDrop spectrophotometer (Thermo Fisher Scientific) and Experion electrophoresis system (Bio-Rad Laboratories). Real-time amplification was performed with RT^2 SYBR Green qPCR Mastermix (Qiagen) using a ViiA 7 Real-Time PCR System (Thermo Fisher Scientific) as described (73). Primers used are shown in *SI Appendix*, Table S1. The expression was calculated by the ddCt method.

Immunohistochemical Staining. Mouse brain was removed from the cranium and divided in the midsagittal plane. The left hemisphere was fixed in 4% formaldehyde for 48 h and embedded in paraffin. Serial sagittal sections (4 μm thick, at 40-μm intervals) spanning the distance between 1.44 and 1.80 mm laterally to the midline/bregma (coordinates according to ref. 74) were prepared. Sections were deparaffinized, subjected to epitope retrieval with Diva Decloaker (Biocare Medical) for 20 min, and blocked with 5% goat or donkey serum. The antibodies were dissolved in Tris-buffered saline supplemented with 0.02% Triton X according to *SI Appendix*, Table S2. The sections were incubated with the primary antibodies at +4 °C overnight, except for the anti-DCX antibody, which was incubated for 72 h. This was followed by incubation with Alexa Fluor-conjugated secondary antibody (*SI Appendix*, Table S2) for 1 h at room temperature. Autofluorescence was blocked with 0.5% Sudan Black B (Sigma) in 70% ethanol for 20 min at room temperature. Nuclei were stained with Hoechst 33342 (NucBlue Live Cell Stain; Thermo Fisher Scientific) for 20 min and mounted with Dako Fluorescence Mounting Medium (Agilent Technologies).

FJC Staining. Deparaffinized sections were primed in 0.06% potassium permanganate for 10 min. FJC (Histo-Chem) was applied in the dark in a concentration of 0.0002% in 0.1% acetic acid for 30 min. The slides were rinsed, air dried, and mounted with DPX (Sigma). A section of a mouse brain 1 wk after neonatal hypoxic–ischemic brain injury (75) was used as positive control.

Confocal Imaging. Fluorescence microscopy was performed using LSM 700 confocal microscope (Carl Zeiss). Areas of interest were captured by software ZEN 2009 (Carl Zeiss). All morphometric analysis was performed on the brain sections blinded for mouse identity. The HC thickness, area, and cell quantification were performed within 13 areas defined in Allen Mouse Brain Atlas (portal.brain-map.org/). Stained cells were analyzed using ImageJ, version 1.0. Objects were measured in 8-bit composite images with threshold adjusted individually for each staining series, to optimize the software's ability to identify individual positive cells. $IGF1R^+$, $pS^{612}IRS1^+$, and DCX^+ cells were counted automatically by the ImageJ software using the Particle Analyzer. $IBA1^+$ microglia and $GFAP^+$ cells were counted manually due to their irregular shape. Morphometric analysis of microglia was performed based on the transformation index of $IBA1^+$ cells, where transformation index above 3 indicated ramified microglia. Markers with high density in the brain tissue, that is, GFAP, IGF1R, and $pS^{612}IRS1$, were counted on one to three sections per mouse per staining; markers that were rare in the tissue, that is, DCX, were counted on three different sections with a distance of 40-μm interval between the sections and averaged. The areas presented are the average of all analyzed sections. To correct for differences in the analyzed areas, we calculated the cell density, defined as the number of cells within each predefined area. Since DCX^+ cells were restricted to the border between the DG_{sg} and DG_{po} areas, the number of DCX^+ cells was normalized to the length of the border.

Serological Analysis. Bioactive IGF1 in serum was analyzed at the Laboratory of Clinical Biochemistry at Sahlgrenska University Hospital. Serum levels of IL-6 and IGF1 were analyzed by ELISA, according to the manufacturer's instructions (IL-6, DY406; R&D Systems for mouse samples; M9316, Sanquin Reagents for human samples; IGF1, DY791; R&D Systems for mouse samples).

Statistical Analysis. Comparison between groups was done pairwise with the Mann–Whitney *U* test. Correlation analyses were performed using Spearman's test. A probability of 0.05 (two-tailed) was used as a significance threshold. Standard software GraphPad Prism (version 6.0; GraphPad Software) was used for statistical analyses.

ACKNOWLEDGMENTS. The authors appreciate the assistance of Drs. Mats Dehlin, Jan Bjersing, and Mitra Nadali (Rheumatology Clinics, Sahlgrenska University Hospital) and Dan Norberg (Rheumatology Unit, Uddevalla Hospital) for clinical evaluation of the patients. We thank Ms. Rowdah Abdalla, Rachelle Espino, and Men Su for technical assistance. This work was supported by the Swedish Research Council (Grants 521-2011-2414 and 521-2014-2637), the Medical Society of Gothenburg, the Swedish Rheumatology Association (Grants R-566961 and R-477321), King Gustaf V's 80-Year Foundation (FAI-2014-0016), Torsten Söderberg's Foundation (2010–2014), Rune and Ulla Amlövs Trust, The Lundberg's Foundation, the regional agreement on medical training and clinical research (ALFGBG-671631). This work used the resources of the UK Medical Bioinformatics Partnership, supported by the UK Medical Research Council (MR/L01632X/1).

1. Covic T, et al. (2012) Depression and anxiety in patients with rheumatoid arthritis: Prevalence rates based on a comparison of the Depression, Anxiety and Stress Scale (DASS) and the Hospital, Anxiety and Depression Scale (HADS). *BMC Psychiatry* 12:6.
2. Matcham F, Ali S, Hotopf M, Chalder T (2015) Psychological correlates of fatigue in rheumatoid arthritis: A systematic review. *Clin Psychol Rev* 39:16–29.
3. Watkins LR, Maier SF (2005) Immune regulation of central nervous system functions: From sickness responses to pathological pain. *J Intern Med* 257:139–155.
4. Druce KL, Jones GT, Macfarlane GJ, Basu N (2015) Determining pathways to improvements in fatigue in rheumatoid arthritis: Results from the British Society for Rheumatology Biologics Register for Rheumatoid Arthritis. *Arthritis Rheumatol* 67: 2303–2310.
5. Cutolo M, Kitas GD, van Riel PL (2014) Burden of disease in treated rheumatoid arthritis patients: Going beyond the joint. *Semin Arthritis Rheum* 43:479–488.
6. Curtis JR, et al. (2013) Patient perspectives on achieving treat-to-target goals: A critical examination of patient-reported outcomes. *Arthritis Care Res (Hoboken)* 65:1707–1712.
7. Hummel T, Schiessl C, Wendler J, Kobal G (2000) Peripheral and central nervous changes in patients with rheumatoid arthritis in response to repetitive painful stimulation. *Int J Psychophysiol* 37:177–183.
8. Flodin P, et al. (2016) Intrinsic brain connectivity in chronic pain: A resting-state fMRI study in patients with rheumatoid arthritis. *Front Hum Neurosci* 10:107.
9. Bekkelund SI, Pierre-Jerome C, Husby G, Mellgren SI (1995) Quantitative cerebral MR in rheumatoid arthritis. *AJNR Am J Neuroradiol* 16:767–772.
10. Wartolowska K, et al. (2012) Structural changes of the brain in rheumatoid arthritis. *Arthritis Rheum* 64:371–379.
11. Boche D, Perry VH, Nicoll JAR (2013) Review: Activation patterns of microglia and their identification in the human brain. *Neuropathol Appl Neurobiol* 39:3–18.
12. Felger JC, Lotrich FE (2013) Inflammatory cytokines in depression: Neurobiological mechanisms and therapeutic implications. *Neuroscience* 246:199–229.
13. Hess A, et al. (2011) Blockade of TNF-α rapidly inhibits pain responses in the central nervous system. *Proc Natl Acad Sci USA* 108:3731–3736.
14. Bas DB, et al. (2012) Collagen antibody-induced arthritis evokes persistent pain with spinal glial involvement and transient prostaglandin dependency. *Arthritis Rheum* 64:3886–3896.
15. Nieto FR, et al. (2016) Neuron-immune mechanisms contribute to pain in early stages of arthritis. *J Neuroinflammation* 13:96.
16. Lampa J, et al. (2012) Peripheral inflammatory disease associated with centrally activated IL-1 system in humans and mice. *Proc Natl Acad Sci USA* 109:12728–12733.

17. Chung CP, et al. (2008) Prevalence of the metabolic syndrome is increased in rheumatoid arthritis and is associated with coronary atherosclerosis. *Atherosclerosis* 196: 756–763.
18. Mirjafari H, et al. (2011) Seropositivity is associated with insulin resistance in patients with early inflammatory polyarthritis: Results from the Norfolk Arthritis Register (NOAR): An observational study. *Arthritis Res Ther* 13:R159.
19. Giles JT, et al. (2015) Insulin resistance in rheumatoid arthritis: Disease-related indicators and associations with the presence and progression of subclinical atherosclerosis. *Arthritis Rheumatol* 67:626–636.
20. Denko CW, Malemud CJ (2005) Role of the growth hormone/insulin-like growth factor-1 paracrine axis in rheumatic diseases. *Semin Arthritis Rheum* 35:24–34.
21. Boström EA, et al. (2011) Resistin and insulin/insulin-like growth factor signaling in rheumatoid arthritis. *Arthritis Rheum* 63:2894–2904.
22. Erlandsson MC, Doria Medina R, Töyrä Silfverswärd S, Bokarewa MI (2016) Smoking functions as a negative regulator of IGF1 and impairs adipokine network in patients with rheumatoid arthritis. *Mediators Inflamm* 2016:3082820.
23. Erlandsson MC, et al. (2017) IGF-1R signalling contributes to IL-6 production and T cell dependent inflammation in rheumatoid arthritis. *Biochim Biophys Acta Mol Basis Dis* 1863:2158–2170.
24. Llorens-Martín M, Torres-Alemán I, Trejo JL (2009) Mechanisms mediating brain plasticity: IGF1 and adult hippocampal neurogenesis. *Neuroscientist* 15:134–148.
25. Nieto-Estévez V, et al. (2016) Brain insulin-like growth factor-I directs the transition from stem cells to mature neurons during postnatal/adult hippocampal neurogenesis. *Stem Cells* 34:2194–2209.
26. Ziegler AN, Levison SW, Wood TL (2015) Insulin and IGF receptor signalling in neural-stem-cell homeostasis. *Nat Rev Endocrinol* 11:161–170.
27. Liu W, Ye P, O'Kusky JR, D'Ercole AJ (2009) Type 1 insulin-like growth factor receptor signaling is essential for the development of the hippocampal formation and dentate gyrus. *J Neurosci Res* 87:2821–2832.
28. Rivera EJ, et al. (2005) Insulin and insulin-like growth factor expression and function deteriorate with progression of Alzheimer's disease: Link to brain reductions in acetylcholine. *J Alzheimers Dis* 8:247–268.
29. Frolich L, et al. (1998) Brain insulin and insulin receptors in aging and sporadic Alzheimer's disease. *J Neural Transm (Vienna)* 105:423–438.
30. Talbot K, et al. (2012) Demonstrated brain insulin resistance in Alzheimer's disease patients is associated with IGF-1 resistance, IRS-1 dysregulation, and cognitive decline. *J Clin Invest* 122:1316–1338.
31. Basta-Kaim A, et al. (2014) Prenatal stress affects insulin-like growth factor-1 (IGF-1) level and IGF-1 receptor phosphorylation in the brain of adult rats. *Eur Neuropsychopharmacol* 24:1546–1556.
32. Roberts RO, et al. (2014) Diabetes and elevated hemoglobin A1c levels are associated with brain hypometabolism but not amyloid accumulation. *J Nucl Med* 55:759–764.
33. McNay EC, Recknagel AK (2011) Brain insulin signaling: A key component of cognitive processes and a potential basis for cognitive impairment in type 2 diabetes. *Neurobiol Learn Mem* 96:432–442.
34. Allen KV, Frier BM, Strachan MW (2004) The relationship between type 2 diabetes and cognitive dysfunction: Longitudinal studies and their methodological limitations. *Eur J Pharmacol* 490:169–175.
35. Bomfim TR, et al. (2012) An anti-diabetes agent protects the mouse brain from defective insulin signaling caused by Alzheimer's disease-associated Aβ oligomers. *J Clin Invest* 122:1339–1353.
36. Hall PE, Lathia JD, Miller NG, Caldwell MA, ffrench-Constant C (2006) Integrins are markers of human neural stem cells. *Stem Cells* 24:2078–2084.
37. McGeer PL, Schulzer M, McGeer EG (1996) Arthritis and anti-inflammatory agents as possible protective factors for Alzheimer's disease: A review of 17 epidemiologic studies. *Neurology* 47:425–432.
38. Sato K (2015) Effects of microglia on neurogenesis. *Glia* 63:1394–1405.
39. Lai KSP, et al. (2017) Peripheral inflammatory markers in Alzheimer's disease: A systematic review and meta-analysis of 175 studies. *J Neurol Neurosurg Psychiatry* 88: 876–882.
40. Bradburn S, Sarginson J, Murgatroyd CA (2018) Association of peripheral interleukin-6 with global cognitive decline in non-demented adults: A meta-analysis of prospective studies. *Front Aging Neurosci* 9:438.
41. Tarkowski E, Andreasen N, Tarkowski A, Blennow K (2003) Intrathecal inflammation precedes development of Alzheimer's disease. *J Neurol Neurosurg Psychiatry* 74: 1200–1205.
42. Ray S, et al. (2007) Classification and prediction of clinical Alzheimer's diagnosis based on plasma signaling proteins. *Nat Med* 13:1359–1362.
43. Weigert C, et al. (2006) Direct cross-talk of interleukin-6 and insulin signal transduction via insulin receptor substrate-1 in skeletal muscle cells. *J Biol Chem* 281: 7060–7067.
44. Kim JA, et al. (2005) Phosphorylation of Ser24 in the pleckstrin homology domain of insulin receptor substrate-1 by mouse pelle-like kinase/interleukin-1 receptor-associated kinase: Cross-talk between inflammatory signaling and insulin signaling that may contribute to insulin resistance. *J Biol Chem* 280:23173–23183.
45. Willette AA, et al. (2015) Association of insulin resistance with cerebral glucose uptake in late middle-aged adults at risk for Alzheimer disease. *JAMA Neurol* 72: 1013–1020.
46. Ekblad LL, et al. (2017) Insulin resistance predicts cognitive decline: An 11-year follow-up of a nationally representative adult population sample. *Diabetes Care* 40:751–758.
47. Lutski M, Weinstein G, Goldbourt U, Tanne D (2017) Insulin resistance and future cognitive performance and cognitive decline in elderly patients with cardiovascular disease. *J Alzheimers Dis* 57:633–643.
48. Kong SH, Park YJ, Lee JY, Cho NH, Moon MK (2018) Insulin resistance is associated with cognitive decline among older Koreans with normal baseline cognitive function: A prospective community-based cohort study. *Sci Rep* 8:650.
49. Voss MW, Vivar C, Kramer AF, van Praag H (2013) Bridging animal and human models of exercise-induced brain plasticity. *Trends Cogn Sci* 17:525–544.
50. Rosano C, et al. (2017) Hippocampal response to a 24-month physical activity intervention in sedentary older adults. *Am J Geriatr Psychiatry* 25:209–217.
51. Kohman RA, DeYoung EK, Bhattacharya TK, Peterson LN, Rhodes JS (2012) Wheel running attenuates microglia proliferation and increases expression of a proneurogenic phenotype in the hippocampus of aged mice. *Brain Behav Immun* 26: 803–810.
52. Maass A, et al. (2016) Relationships of peripheral IGF-1, VEGF and BDNF levels to exercise-related changes in memory, hippocampal perfusion and volumes in older adults. *Neuroimage* 131:142–154.
53. Vukovic J, Colditz MJ, Blackmore DG, Ruitenberg MJ, Bartlett PF (2012) Microglia modulate hippocampal neural precursor activity in response to exercise and aging. *J Neurosci* 32:6435–6443.
54. Bender F, et al. (2015) Theta oscillations regulate the speed of locomotion via a hippocampus to lateral septum pathway. *Nat Commun* 6:8521.
55. Kang KY, et al. (2013) Metformin downregulates Th17 cells differentiation and attenuates murine autoimmune arthritis. *Int Immunopharmacol* 16:85–92.
56. Marder W, et al. (2013) The peroxisome proliferator activated receptor-γ pioglitazone improves vascular function and decreases disease activity in patients with rheumatoid arthritis. *J Am Heart Assoc* 2:e000441.
57. Ormseth MJ, et al. (2013) Peroxisome proliferator-activated receptor γ agonist effect on rheumatoid arthritis: A randomized controlled trial. *Arthritis Res Ther* 15:R110.
58. Du LL, et al. (2015) AMPK activation ameliorates Alzheimer's disease-like pathology and spatial memory impairment in a streptozotocin-induced Alzheimer's disease model in rats. *J Alzheimers Dis* 43:775–784.
59. Rajasekar N, Nath C, Hanif K, Shukla R (2017) Intranasal insulin administration ameliorates streptozotocin (ICV)-induced insulin receptor dysfunction, neuroinflammation, amyloidogenesis, and memory impairment in rats. *Mol Neurobiol* 54: 6507–6522.
60. Melemedjian OK, et al. (2011) Targeting adenosine monophosphate-activated protein kinase (AMPK) in preclinical models reveals a potential mechanism for the treatment of neuropathic pain. *Mol Pain* 7:70.
61. Burton MD, et al. (2017) Pharmacological activation of AMPK inhibits incision-evoked mechanical hypersensitivity and the development of hyperalgesic priming in mice. *Neuroscience* 359:119–129.
62. Byrne FM, Cheetham S, Vickers S, Chapman V (2015) Characterisation of pain responses in the high fat diet/streptozotocin model of diabetes and the analgesic effects of antidiabetic treatments. *J Diabetes Res* 2015:752481.
63. Wolfe F, et al. (1990) The American College of Rheumatology 1990 criteria for the classification of fibromyalgia. Report of the Multicenter Criteria Committee. *Arthritis Rheum* 33:160–172.
64. Hedin PJ, Hamne M, Burckhardt CS, Engström-Laurent A (1995) The Fibromyalgia Impact Questionnaire, a Swedish translation of a new tool for evaluation of the fibromyalgia patient. *Scand J Rheumatol* 24:69–75.
65. Pincus T, Summey JA, Soraci SA, Jr, Wallston KA, Hummon NP (1983) Assessment of patient satisfaction in activities of daily living using a modified Stanford Health Assessment Questionnaire. *Arthritis Rheum* 26:1346–1353.
66. Tustison NJ, et al. (2010) N4ITK: Improved N3 bias correction. *IEEE Trans Med Imaging* 29:1310–1320.
67. Heckemann RA, et al. (2015) Brain extraction using label propagation and group agreement: Pincram. *PLoS One* 10:e0129211.
68. Heckemann RA, et al.; Alzheimer's Disease Neuroimaging Initiative (2010) Improving intersubject image registration using tissue-class information benefits robustness and accuracy of multi-atlas based anatomical segmentation. *Neuroimage* 51:221–227.
69. Hammers A, et al. (2003) Three-dimensional maximum probability atlas of the human brain, with particular reference to the temporal lobe. *Hum Brain Mapp* 19: 224–247.
70. Brand DD, Latham KA, Rosloniec EF (2007) Collagen-induced arthritis. *Nat Protoc* 2: 1269–1275.
71. Andersson KM, Svensson MN, Erlandsson MC, Jonsson IM, Bokarewa MI (2015) Down-regulation of survivin alleviates experimental arthritis. *J Leukoc Biol* 97:135–145.
72. Olmarker K, Størkson R, Berge OG (2002) Pathogenesis of sciatic pain: A study of spontaneous behavior in rats exposed to experimental disc herniation. *Spine* 27: 1312–1317.
73. Erlandsson MC, et al. (2013) Expression of metastasin S100A4 is essential for bone resorption and regulates osteoclast function. *Biochim Biophys Acta* 1833:2653–2663.
74. Paxinos G, Franklin K (2012) *Paxinos and Franklin's the Mouse Brain in Stereotaxic Coordinates* (Academic, San Diego), 4th Ed.
75. Morán J, et al. (2017) Intranasal C3a treatment ameliorates cognitive impairment in a mouse model of neonatal hypoxic-ischemic brain injury. *Exp Neurol* 290:74–84.